Available online at www.sciencedirect.com
ScienceDirect
Journal of Natural Gas Chemistry 19(2010)362–368
Journal of Natural Gas Chemistry
www.elsevier.com/locate/jngc

Kinetics of the water-gas shift reaction in Fischer-Tropsch synthesis over a nano-structured iron catalyst

Ali Nakhaei Pour[1,2*], Mohammad Reza Housaindokht[1], Sayyed Faramarz Tayyari[1], Jamshid Zarkesh[2]

1. Department of Chemistry, Ferdowsi university of Mashhad, P. O. Box: 91775-1436, Mashhad, Iran;
2. Research Institute of Petroleum Industry of National Iranian Oil Company, P. O. Box: 14665-137, Tehran, Iran

[Manuscript received November 2, 2009; revised December 21, 2009]

Abstract
Based on formate and direct oxidation mechanisms, three Langmuir-Hinshelwood-Hougen-Watson (LHHW) kinetic models of the water-gas-shift (WGS) reaction over a nano-structured iron catalyst under Fischer-Tropsch synthesis (FTS) reaction conditions were derived and compared with those over the conventional catalyst. The conventional and nanostructured Fe/Cu/La/Si catalysts were prepared by co-precipitation of Fe and Cu nitrates in aqueous media and water-oil micro-emulsion, respectively. The WGS kinetic data were measured by experiments over a wide range of reaction conditions and comparisons were also made for various rate equations. WGS rate expressions based on the formate mechanism with the assumption that the formation of formate is rate determining step were found to be the best.

Key words
kinetics; water-gas-shift reaction; iron catalyst; Fischer-Tropsch synthesis

1. Introduction

Iron-based catalysts are preferred to cobalt-based counterparts in Fischer-Tropsch synthesis (FTS) of hydrocarbons from coal or biomass-derived synthesis gas because of their lower cost, lower methane selectivity, lower sensitivity to poisons, flexible product, and robustness at low H_2/CO ratios (bossessing high activity for production of H_2 via the water-gas-shift reaction) [1−3]. The water-gas-shift (WGS) reaction can be shown as:

$$CO + H_2O \longleftrightarrow CO_2 + H_2 \quad (1)$$

WGS reaction is a reversible reaction with respect to CO and assumed that carbon dioxide is essentially formed by this reaction [4−8]. It is generally accepted that FTS and WGS reactions take place on different active sites over a precipitated iron catalyst and the two reactions will only influence each other via the gas phase. Literature suggests that the formation of iron carbides results in a high FTS activity, and the magnetite (Fe_3O_4) is the most active phase for WGS reaction [9−13]. Thus the FTS (hydrocarbon formation) and WGS (carbon dioxide formation) reactions can be described with separate kinetic expressions.

Recent studies showed that nanosized iron particles were essential to achieve high FTS activity. Some authors prepared supported iron-based Fischer-Tropsch catalysts by micro-emulsion method, and reported high activity and selectivity to oxygenates [14−18]. A micro-emulsion is optically transparent and has a thermodynamically stable dispersion of water phase into an organic phase stabilized by a surfactant [19].

The objective of this work is to establish systematically and compare Lagmuir-Hinshelwood-Hogen-Watson (LHHW) kinetics model for the WGS reaction on the basis of possible detailed mechanism over a nanostructured Fe/Cu/La/Si catalyst under FTS reaction conditions with that over conventional catalyst. Using the experimental data, three WGS kinetics models are presented and compared separately.

2. Experimental

2.1. Catalyst preparation

Fe/Cu/La conventional catalyst was prepared by co-precipitation of Fe and Cu nitrates at a constant pH to form porous Fe-Cu oxyhydroxide powders. Catalyst precursor was promoted by impregnation with La $(NO_3)_3$ solution and treatment in air as described previously [6−8].

* Corresponding author. Tel/Fax: +98-21-44739716; Email: nakhaeipoura@ripi.ir and nakhaeipoura@yahoo.com

doi:10.1016/S1003-9953(09)60085-2

Fe/Cu/La nano-catalyst precursors were prepared by co precipitation in a water-in-oil micro-emulsion as described previously [14,15]. The catalysts were dried at 383 K for 16 h and calcined at 773 K for 3 h in air. The catalyst compositions were designed in terms of the atomic ratios as: 100Fe/5.64Cu/2La/19Si and labeled as conv. and nano catalysts. Based on previous results, the particle sizes of the conv. and nano catalysts were determined to be 0.5 μm and 20 nm, respectively [14,15].

2.2. Catalytic performance

Steady-state FTS and WGS reaction rates and selectivities were measured in a continuous spinning basket reactor (stainless steel, $H = 0.122$ m, $D_o = 0.052$ m, $D_i = 0.046$ m) with temperature controllers (WEST series 3800). A J-type movable thermocouple made it possible to monitor the bed temperature axially, which was within ± 0.5 K of the average bed temperature. The reactor system also included a 50 cm^3 stainless steel cold trap at ambient temperature located before the gas chromatograph sampling valve. Non-condensable gases passed through sampling valve into an online gas chromatograph continuously then vented through a soap-film bubble meter. Separate Brooks 5850 mass flow controllers were used to add H_2 and CO at a desired rate to admixing vessel that was preceded by a palladium trap and a molecular sieve trap to remove metal carbonyls and water before entering the reactor. A compact pressure controller was used to control the pressure. The flow rate of tail gas was measured by a wet gas meter.

Blank experiments showed that the spinning basket reactor charged with inert silica sand without the catalyst gave no conversion of syngas. The fresh catalyst was crushed and sieved to particles with the diameter of 0.25–0.36 mm (40–60 ASTM mesh). The weight of the catalyst loaded was 2.5 g and diluted by 30 cm^3 inert silica sand with the same mesh size range. The catalyst samples were activated by a 5% (v/v) H_2/N_2 gas mixture with space velocity of 15.1 $nl \cdot h^{-1} \cdot g_{Fe}^{-1}$ at 0.1 MPa and 1800 rpm. The reactor temperature increased to 673 K with a heating rate of 5 K/min, maintained for 1 h at this temperature, and then reduced to 543 K. The activation was followed by the synthesis gas stream with $H_2/CO = 1$ and space velocity of 3.07 $nl \cdot h^{-1} \cdot g_{Fe}^{-1}$ for 24 h in 0.1 MPa and 543 K before setting the actual reaction temperature and pressure. After catalyst reduction, synthesis gas was fed to the reactor under conditions of 563 K, 1.7 MPa, (H_2/CO) feed = 1 and a space velocity of 10.4 $nl \cdot h^{-1} \cdot g_{Fe}^{-1}$. A stabilization period of 15 h was conducted under the reaction conditions, and then the kinetics measurement was carried out. After changing the process conditions, at least 12 h were used for the system stabilization before a new mass balance period. After reaching steady activity and selectivity, the kinetics of the Fischer-Tropsch synthesis was measured.

The external mass transfer limitation was investigated by comparing the CO conversions under different stirring speeds of the reactor (data not shown). All our experiments were carried out at 1800 rpm which was safe to eliminate the external mass transfer limitations under all kinetic conditions.

During the entire runs, the reactor temperature varied between 543 and 593 K, the pressure was 1.7 MPa, and the space velocity of the synthesis gas varied between 3.5 and 28.7 $nl \cdot h^{-1} \cdot g_{Fe}^{-1}$. The H_2/CO ratio of the feed was kept constant in all space velocities. Periodically during the run, the catalyst activity was measured under a preset "standard" condition (a space velocity equal to 10.4 $nl \cdot h^{-1} \cdot g_{Fe}^{-1}$) to check the catalyst deactivation. The water partial pressure was determined by collecting the water in the trap, separating it from the oil, and weighing. The weight of water was converted to partial pressure in the reactor based on the ideal gas law.

The products were analyzed by means of three-gas-chromatograph, a Shimadzu 4C gas chromatograph equipped with two subsequently connected packed columns: Porapak Q and Molecular Sieve 5A, and a thermal conductivity detector (TCD) with Ar as carrier gas was used for hydrogen analysis. A Varian CP 3800 with a chromosorb column and a thermal conductivity detector (TCD) was used to analyze CO, CO_2, CH_4, and other non-condensable gases. A Varian CP 3800 with a Petrocol^{Tm} DH100 fused silica capillary column and a flame ionization detector (FID) was used for organic liquid products so that a complete product analysis distribution could be provided.

3. Results and discussion

3.1. Kinetic models

Two mechanisms have been proposed for the WGS reaction over metal oxide catalysts in a non-FT environment: formate and direct oxidation mechanisms [9,10,13]. The direct oxidation mechanism comprises oxidation-reduction cycles. In this mechanism it is assumed that water is adsorbed and dissociated on the reduced sites to produce hydrogen while the sites are oxidized. In the following step, CO is oxidized to CO_2 and the oxidized sites are reduced to complete the cycle. In the other mechanism, it is assumed that adsorbed intermediate (possibly a formate species) is formed through reaction between carbon monoxide and a hydroxyl species or water, which then decomposes to H_2 and CO_2. The hydroxyl intermediate is formed via decomposition of water.

On the basis of the formate intermediate (WGS I, WGS II) and direct oxidation mechanism (WGS III) for the WGS reaction, three sets of elementary reactions for the WGS reaction were derived in this work, and are listed in Table 1. For the derivation of the rate expressions, the WGS reaction and the FTS reaction (hydrocarbon formation) are assumed to proceed on different active sites, and one rate-determining step is assumed in the sequence of WGS elementary reactions. The remaining steps can be considered to be at quasi-equilibrium and other steps are regarded as fast reversible processes, for which the equilibrium assumption can be used. On the basis of the mentioned assumptions, three kinetic rate equations

were developed and the expressions are given in Table 2. In these rate equations, P_j is the partial pressure of species j in the effluent stream and K_p is the equilibrium constant of the WGS reaction.

For the temperature dependency of the equilibrium constant of the WGS reaction, the following relation was used [10]:

$$\log K_p = \left(\frac{P_{CO_2} P_{H_2}}{P_{CO} P_{H_2O}}\right)_{eq,T} = \left(\frac{2073}{T} - 2.029\right) \quad (2)$$

where K_p is the WGS equilibrium constant at temperature T. The reaction rate of CO_2 was calculated from a material balance over the reactor, assuming ideal gas behavior. Normalizing the concentrations of all the intermediates in formate mechanisms on the catalyst surface leads to:

$$[s] + [Hs] + [COs] + [H_2Os] + [OHs] + [COOHs] = 1 \quad (3)$$

Based on previous knowledge of adsorbed spices on the magnetite sites, some simplifications can be considered in achieving the rate expression equations (Table 2). In the first kinetic expression (WGS I), it is assumed that the adsorption of H_2, OH and CO_2 relative to CO and H_2O is negligible and the formation of formate intermediate is rate determining step. In the second model (WGS II) it is assumed that H_2O was being dissociatively adsorbed, the formation of formate intermediate (reaction Step 6) was rate determining step and the adsorption of H_2, H_2O and CO_2 is negligible relative to CO and OH.

Table 1. Elementary reaction steps for WGS reaction

Model		Reaction step	Elementary reaction
WGS I	1		CO+s ⟷ COs
	2		CO_2+s ⟷ CO_2s
	3		H_2O+s ⟷ H_2Os
	4		H_2+2s ⟷ 2Hs
	5	rate determining step	COs+H_2Os ⟷ HCOOs+Hs
	6		HCOOs+s ⟷ Hs+CO_2s
WGS II	1		CO+s ⟷ COs
	2		CO_2+s ⟷ CO_2s
	3		H_2O+s ⟷ H_2Os
	4		H_2Os+s ⟷ OHs+Hs
	5		H_2+2s ⟷ 2Hs
	6	rate determining step	COs+OHs ⟷ HCOOs+s
	7		HCOOs+s ⟷ Hs+CO_2s
WGS III	1		CO+s ⟷ COs
	2		H_2+2s ⟷ 2Hs
	3		H_2O+2s ⟷ OHs+Hs
	4		OHs+s ⟷ Os+Hs
	5		COs+Os ⟷ CO_2s+s
	6	rate determining step	CO_2s ⟷ CO_2+s

Table 2. Rate expressions considered for the WGS reaction, R_{CO_2} (mmol·g_{cat}^{-1}·s^{-1})

Model	Kinetic equation	Site balance
WGS I	$R_{CO_2} = k_w(P_{CO}P_{H_2O} - P_{CO_2}P_{H_2}/K_P)/(1+K_1P_{CO}+K_3P_{H_2O})^2$	s+COs+H_2Os
	$k_w = k_5K_1K_3$(mmol·g_{cat}^{-1}·s^{-1}·bar^{-2})	
WGS II	$R_{CO_2} = k_w(P_{CO}P_{H_2O}/P_{H_2}^{1/2} - P_{CO_2}P_{H_2}^{1/2}/K_P)/(1+K_1P_{CO}+KP_{H_2O}/P_{H_2}^{1/2})^2$	s+COs+OHs
	$k_w = k_5K_1K_3K_4K_5^{-1/2}$(mmol·$g_{cat}^{-1}$·$s^{-1}$·$bar^{-3/2}$)	
	$K = K_4K_3/K_5^{1/2}$	
WGS III	$R_{CO_2} = k_w(P_{CO}P_{H_2O}/P_{H_2} - P_{CO_2}/K_P)/(1+KP_{CO}P_{H_2O}/P_{H_2})$	s+CO_2s
	$k_w = k_6K_1K_2^{-1/2}K_3K_4K_5$(mmol·$g_{cat}^{-1}$·$s^{-1}$·$bar^{-1}$)	

Model WGS III is based on oxidation-reduction mechanism. In this series of reactions, based on thermodynamics consideration, CO_2 desorption reaction (reaction Step 6) can be regarded as rate determining step and the adsorbed species [CO_2s] must be dominant. Based on this assumption, the kinetics expression of WGS III was obtained.

The model parameters were calculated from the experimental data by minimizing the χ^2 function with the Levenberg-Marquardt (LM) algorithm, with all experimental reaction rates [20]:

$$\chi^2 = \sum \frac{(R_{exp} - R_{cal})^2}{\delta^2} \quad (4)$$

where, δ^2 is the relative variance of the experimental selectivities in the WGS reaction rate. In this approach, the difference between the measured and predicted rates is divided by the standard deviation of the involved rate measurement. Data points with a high accuracy have low standard deviations and therefore count more heavily toward the sum of errors than inaccurate data. In other words, the weight (importance) assigned to each observation is related to the accuracy of that specific measurement. The variance is due to experimental inaccuracies and lack of fit of the kinetic model. Confidence limits on the estimated model parameters were calculated at a 95% confidence level. Whereas the value of chi-square was used for model optimization and discrimination, the mean absolute relative residual (MARR) is reported as a measure of the goodness of fit:

$$\text{MARR} = 100\sum_1^n \left|\left(\frac{R_{exp} - R_{cal}}{R_{exp}}\right)\right| \frac{1}{n} \quad (5)$$

where, n is the number of data points included. The estimates of the kinetic parameters must have physical relevance. Rate models yielding negative adsorption coefficients were excluded for further model discrimination. Furthermore, the surface fractions of adsorbed species should be realistic and

the residuals between model and experiment should be normally distributed with zero average. The discrimination between the rival models and the estimation of the parameter values was performed using the experiments at 563 K.

3.2. Isothermal discrimination

The WGS reaction rate was optimized with the kinetic expressions in Table 2. The corresponding model parameters and related MARR value and weighted sum of errors (χ^2-value) for conventional and nano catalysts are also given in Tables 3 and 4, respectively. In these Tables, K_1, K_3, and K parameters are related to adsorption coefficients of CO, H_2O, and hydroxyl groups for WGS I and WGS II expressions, respectively. However, K parameter in WGS III expression is related to adsorption coefficients of adsorbed CO_2 in rate determining step. It should further be noted that the adsorption coefficients of CO or CO containing intermediates are small compared to the adsorption coefficients of water or hydroxyl groups. This is in agreement with the findings of other studies on the WGS reaction in the iron-based FTS reactions [10,21]. It is found from Tables 3 and 4 that the WGS kinetic model obtained from the formate mechanism is better in fitting the experimental data than the model obtained from the direct oxidation mechanism. A possible explanation is that the dissociation of hydroxyl intermediate to the adsorbed oxygen and hydrogen is not energetically favorable under FTS reaction conditions. This is also supported by quantum chemical calculation on transition metals, which shows that the hydroxyl dissociation is energetically unfavorable with a relatively high activation barrier [22,23]. According to the MARR value and weighted sum of errors (χ^2-value) in Table 3, the WGS I model (based on the formate mechanism) showed better data fitting for both catalysts.

An estimate of the extent of the water-gas shift reaction can be obtained by the following WGS reaction quotient (RQ_{WGS}) [24]:

$$RQ_{\mathrm{WGS}} = \frac{P_{\mathrm{CO_2}} P_{\mathrm{H_2}}}{P_{\mathrm{CO}} P_{\mathrm{H_2O}}} \tag{6}$$

The approach to the WGS equilibrium can be described through the parameter η, obtained through dividing the WGS reaction quotient by the equilibrium constant at the reaction temperature [21,22]:

$$\eta = \frac{1}{K_p}\left(\frac{P_{\mathrm{CO_2}} P_{\mathrm{H_2}}}{P_{\mathrm{CO}} P_{\mathrm{H_2O}}}\right) \tag{7}$$

The value of η ranged from 0 to 1, the latter being the equilibrium value [25]. In general, the value of η was small at low carbon monoxide conversions and increased at higher carbon monoxide conversions [13,21,22]. This indicates that the WGS reaction under FTS reaction conditions is far from equilibrium, which was also observed by others [13,21,22].

Table 3. WGS kinetics model parameters for nano catalyst

Model	Kinetic parameters	χ^2	MARR (%)
WGS I	$k_w = 0.21$ mmol·g_{cat}^{-1}·s^{-1}·bar^{-2}	870	8.73
	$K_1 = 0.39$ bar^{-1}, $K_3 = 3.54$ bar^{-1}		
WGS II	$k_w = 1.20$ mmol·g_{cat}^{-1}·s^{-1}·$bar^{-3/2}$	984	9.15
	$K_1 = 0.60$ bar^{-1}, K = 5.51 bar^{-1}		
WGSIII	$k_w = 0.12$ mmol·g_{cat}^{-1}·s^{-1}·bar^{-1}	2750	21.94
	$K = 1.92$ bar^{-1}		

Table 4. WGS kinetics model parameters for conventional catalyst

Model	Kinetic parameters	χ^2	MARR (%)
WGS I	$k_w = 0.25$ mmol·g_{cat}^{-1}·s^{-1}·bar^{-2}	978	9.85
	$K_1 = 0.39$ bar^{-1}, $K_3 = 3.54$ bar^{-1}		
WGS II	$k_w = 1.21$ mmol·g_{cat}^{-1}·s^{-1}·$bar^{-3/2}$	1184	10.15
	$K_1 = 0.59$ bar^{-1}, $K = 12.69$ bar^{-1}		
WGSIII	$k_w = 0.12$ mmol·g_{cat}^{-1}·s^{-1}·bar^{-1}	2350	17.94
	$K = 3.68$ bar^{-1}		

In order to check the systematic isothermal discrimination, the agreement between each of the rival rate equations and the measured reaction rates was presented as a function of the approach to WGS equilibrium. Figure 1 shows that the errors in the prediction of WGS considered models with the approach to equilibrium, suggesting a systematic deviation in the models based on oxidation-reduction cycles which may be indicative of a fundamental incorrectness in these expressions. On the contrary, the deviations in the models based on the formate mechanism appear to be randomly scattered rather than consistent errors. As shown in this Figure, at higher approach to WGS equilibrium (η), deviation from unit in all models was increased. It is known that the WGS reaction occurs on different type of sites as compared with FTS reaction and the two reactions will only influence each other via the gas phase concentrations of the reactants. However, the FTS reaction must depend increasingly on the hydrogen formed by the WGS reaction as the carbon monoxide conversion increases. Thus, the overall FTS rate is increasingly affected by the rate/extent of the WGS reaction at high conversions and the deviation from unit in all models may be related to this conjugation of FTS and WGS reactions [24].

Figure 2 compares the experimental and calculated WGS reaction rates of assumed models. In this Figure, R^2 is a parameter for discrimination of results and it is compared by calculated and experimental WGS reaction rates and defined as:

$$R^2 = 1 - \frac{\text{Residual sum of squares}}{\text{Corrected sum of squares}} \tag{8}$$

As shown in this Figure, the reaction expression of WGS I shows the largest value of R^2 and so is the best model for fitting the experimental data among the three models introduced in Table 1. Reaction rate expression of WGS I is similar to the optimal model of van der Laan and Beenackers [9]. This model assumes that the rate of the WGS reaction is determined by the reaction of adsorbed carbon monoxide and hydroxyl toward a formate intermediate and the adsorptions of CO and water were dominated in the site balance. WGS II

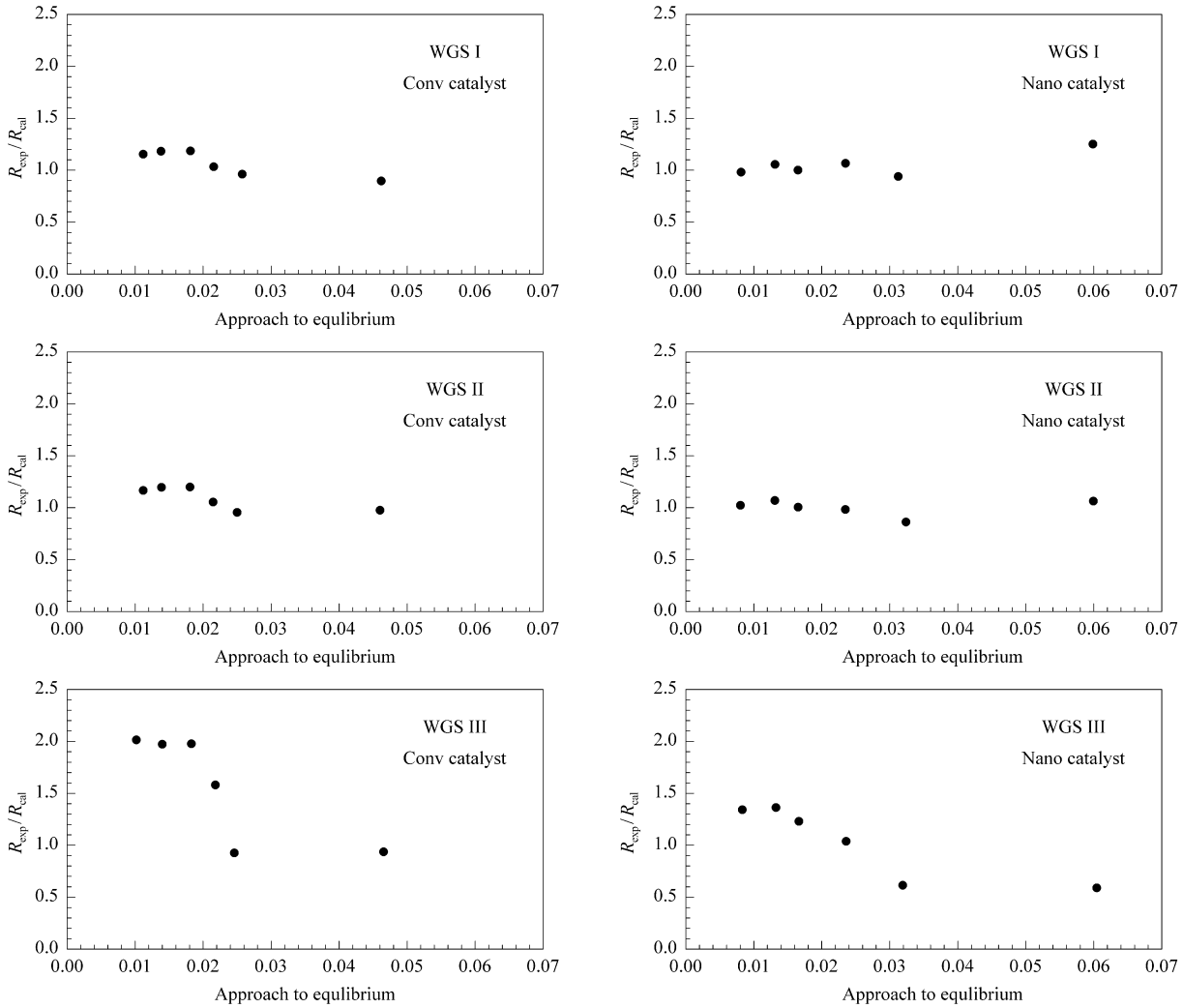

Figure 1. Comparison of the calculated and experimental CO_2 flow rates (mmol·g_{cat}^{-1}·s^{-1}) as the WGS reaction approaches equilibrium

model assumes that the rate of the WGS reaction is determined by the reaction of adsorbed carbon monoxide and hydroxyl toward a formate intermediate. In the reaction rate expression of WGS II, it is assumed that adsorptions of CO and hydroxyl species were dominated in the site balance which are present in the rate determining step. It should also be noted from Table 3 that the adsorption coefficients of CO or CO containing intermediates are small compared with the the adsorption coefficients of water or hydroxyl groups and the adsorption coefficient of hydroxyl groups is higher than that of water.

3.3. Calculation of WGS activation energy

WGS I model is the best model for both catalysts, so we used this model for evaluation of WGS activation energy at various temperatures. Table 5 lists the calculated WGS reaction rate constants (k_w) for conventional and nano catalysts at various temperatures. These results indicated that by decreasing the catalyst particle size from conventional to nano catalyst, WGS reaction rate constants (k_w) decreased and as a result the WGS activity of catalysts decreased. The temperature dependence of the reaction rate constants is evaluated according to the Arrhenius-type equation:

$$k_w(T) = Aexp(-Ea/RT) \quad (9)$$

The activation energies are calculated to be about 70 and 81 kJ/mol for conventional and nano catalysts, respectively, and are listed in Table 5. These results indicated that the activation energy and rate of WGS reaction increased and as a result, WGS reaction rate decreased by decreasing the catalyst particle size. These calculated values of activation energy indicate that while the WGS reaction occurs on different type of sites as compared with FTS reaction, both these reactions will influence each other via the gas phase concentrations of reactants and WGS reaction is active in FTS reaction system [11,21].

Table 5. WGS kinetics data obtained from the WGS I model

Catalyst	k_w(mmol·g_{cat}^{-1}·s^{-1}·bar^{-2})			E_a (kJ/mol)
	543 K	563 K	593 K	
Nano catalyst	0.12	0.20	0.54	81
Conv. catalyst	0.18	0.25	0.65	70

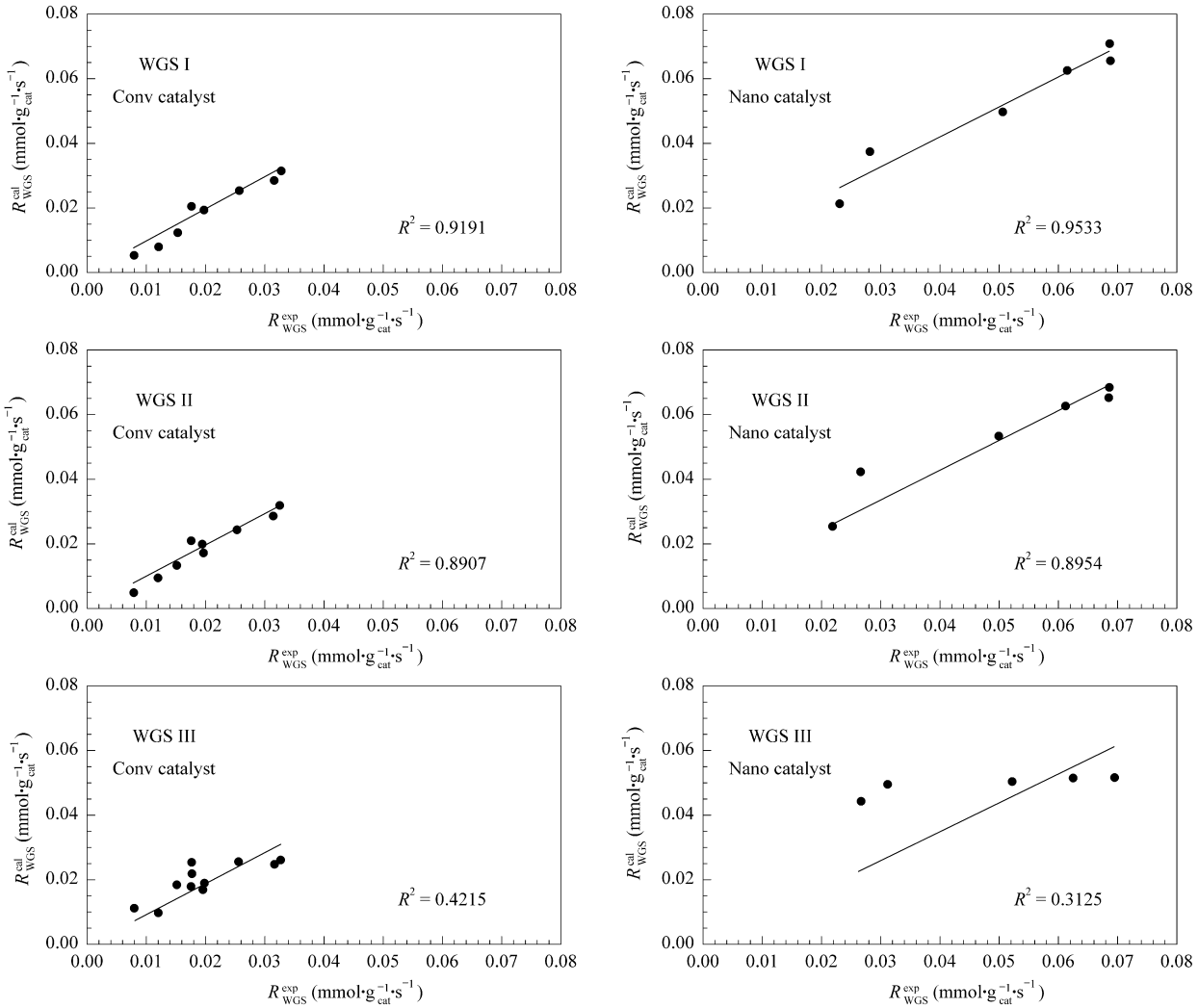

Figure 2. Comparison between calculated and experimental CO_2 flow rates. R^2 = 1–(residual sum of squares)/(corrected sum of squares)

Botes [21] reported that WGS sites are mainly covered with water and/or hydroxyl species in the Fe-low-temperature FT synthesis. This is different from the findings in this work. Results in the present work show that with increasing the temperatures in FT reaction the concentration of CO adsorbed on the WGS catalytic sites was increased and must be considered in reaction rate expression as the results reported by van der Laan and Beenackers [10].

4. Conclusions

Three Langmuir-Hinshelwood-Hougen-Watson type rate equations were derived on the basis of formate and direct oxidation mechanisms. WGS rate expression based on the formate mechanism was found to provide an improved description of the WGS kinetic data. These results indicated that by decreasing the catalyst particle size, the activation energy of WGS reaction increased and as a result, the reaction rate decreased consequently.

References

[1] Anderson R B. The Fischer-Tropsch Synthesis. Orlando: Academic Press, 1984
[2] Bartholomew C H. Recent Developments in Fischer-Tropsch Catalysis, New Trends in CO Activation, Studies in Surface Science and Catalysis, No. 64, Amsterdam: Elsevier, 1991
[3] Dry M E. In: Anderson J R, Bourdart M eds. Catalysis Sciences and Technology, Vol 1. New York: Springer-Verlag, 1981
[4] Jothimurugesan K, GoodwinJr J G, Gangwal S K, Spivey J J. *Catal Today*, 2000, 58: 335
[5] Jin Y M, Datye A K. *J Catal*, 2000, 196: 8
[6] Pour A N, Shahri S M K, Zamani Y, Irani M, Tehrani S. *J Natur Gas Chem*, 2008, 17: 242
[7] Pour A N, Zamani Y, Tavasoli A, Shahri S M K, Taheri S A. *Fuel*, 2008, 87: 2004
[8] Pour A N, Shahri S M K, Bozorgzadeh H R, Zamani Y, Tavasoli A, Marvast M A. *Appl Catal A*, 2008, 348: 201
[9] Van Der Laan G P, Beenackers A A C M. *Catal Rev Sci Eng*, 1999, 41: 255
[10] van der Laan G P, Beenackers A A C M. *Appl Catal A*, 2000, 193: 39

[11] Wang Y N, Ma W P, Lu Y J, Yang J, Xu Y Y, Xiang H W, Li Y W, Zhao Y L, Zhang B J. *Fuel*, 2003, 82: 195
[12] Guo X H, Liu Y, Chang J, Bai L, Xu Y Y, Xiang H W, Li Y W. *J Natur Gas Chem*, 2006, 15: 105
[13] Teng B T, Chang J, Yang J, Wang G, Zhang C H, Xu Y Y, Xiang H W, Li Y W. *Fuel*, 2005, 84: 917
[14] Pour A N, Taghipoor S, Shekarriz M, Shahri S M K, Zamani Y. *J Nanosci Nanotech*, 2009, 9: 4425
[15] Pour A N, Housaindokht M R, Tayyari S F, Zarkesh J. *J Natur Gas Chem*, 2010, 19: 107
[16] Sarkar A, Seth D, Dozier A K, Neathery J K, Hamdeh H H, Davis B H. *Catal Lett*, 2007, 117: 1
[17] Herranz T, Rojas S, Pérez-Alonso F J, Ojeda M, Terreros P, Fierro J L G. *Appl Catal A*, 2006, 311: 66
[18] Eriksson S, Nylén U, Rojas S, Boutonnet M. *Appl Catal A*, 2004, 265: 207
[19] Schwuger M J, Stickdorn K, Schomaecker R. *Chem Rev*, 1995, 95: 849
[20] Press W H, Flannery B P, Teukolsky S A, Vetterling W T. Numerical Recipes in Pascal. New York: Cambridge University Press, 1989
[21] Botes F G. *Appl Catal A*, 2007, 328: 237
[22] Krishnamoorthy S, Li A W, Iglesia E. *Catal Lett*, 2002, 80: 77
[23] Wu B S, Bai L, Xiang H W, Li Y W, Zhang Z X, Zhong B. *Fuel*, 2004, 83: 205
[24] Raje A P, O'Brien R J, Davis B H. *J Catal*, 1998, 180: 36
[25] Michaelides A, Hu P. *J Am Chem Soc*, 2001, 123: 4235

"SCI Impact Factor 2009" being 0.95 for *Journal of Natural Gas Chemistry*

The "SCI impact factor" of *Journal of Natural Gas Chemistry (JNGC)* is 0.95, according to the "2009 Journal Citation Reports (JCR) Science Edition".

Since 2007, *JNGC* has been included in the Science Citation Index Expanded (SCI-E), the Chemistry Citation Index and the Journal Citation Reports/Science Edition, all published by Thomson Scientific, and this is the first time that an impact factor has been assessed for *JNGC* by the Journal Citation Reports.

We would like to take this opportunity to express our sincere thanks to all members of the editorial board, to all authors and contributors, as well as to all reviewers and readers for your great contributions to the Journal during the past years. We also appreciate deeply the efforts and assistance of the Elsevier distributor. We hope that with your continuous and ever-increasing supports and concerns, the *Journal of Natural Gas Chemistry* will become a significant journal in the field of energy chemistry in general, and in the field of natural gas in particular, in the near future.

Editorial Office
Journal of Natural Gas Chemistry